Enhancing Open-Circuit Voltage in Dye-Sensitized Solar Cells through TiO_2 Nanoparticles Composite with ZnO

Somnath Middya*
Assistant Professor
Department of Physics
Bankim Sardar College, South 24 Parganas, West Bengal, India

1. Introduction

Titanium dioxide holds significance due to its distinctive electronic and optical properties, prompting extensive investigation. With attributes like high oxidation power, non-toxicity, long-term stability, and low synthesis cost, it emerges as a promising inorganic material. Despite its challenge in harvesting the visible solar spectrum due to a larger band gap, significant efforts have been invested by scientists to make it applicable in photovoltaic devices. Various attempts have been made to enhance its absorption efficiency under visible light by doping with transition elements (Zn, Ni, Co, Mn, Sn) [1-3] and group elements (N, C, B, S, P) [4,5]. Recent focus on doping TiO2 with halogens, particularly fluorine, has proven efficient in advancing photovoltaic research by improving absorption in the UV-VIS region and reducing the band gap energy [6].

The active performance of titanium dioxide (TiO2) nanoparticles in photovoltaics and electronic devices, with diverse architectures, has been successfully explored. Dye Sensitized Solar Cells (DSSC) within the photovoltaic family show promise due to their use of low-cost materials and simplified manufacturing processes, offering reasonable energy-conversion efficiency. However, challenges persist, such as the recombination of photo-injected electrons in the conduction band of TiO2 with oxidized dye. The relatively slow electron transport rate, resulting from multiple trapping/detrapping events within grain boundaries, leads to high interface recombination, limiting device efficiency. In DSSC, the small individual particle size prevents the formation of a space charge region, indicating a high recombination rate of photo-injected electrons due to the absence of an energy barrier at the electrode/electrolyte interface [10]. A literature survey reveals systematic efforts to reduce recombination at the interface, including the formation of bilayers, composites, and passivation by electro polymerization [11].

A typical Dye Sensitized Solar Cell (DSSC) comprises a transparent conducting oxide layer situated on a glass substrate, a layer of dye-sensitized oxide semiconductor nanoparticles (predominantly TiO_2), a liquid redox electrolyte, and a counter electrode [12,13]. Titanium oxide (TiO_2) nanoparticles have gained prominence as a superior material for DSSC applications due to their wide band gap and n-type semiconducting properties [14]. The performance of DSSC is intricately linked to factors such as morphology, size, dimension, and doping concentration, which determine electrical, thermal, optical, and mechanical properties [15]. Reported efficiencies for TiO_2-based DSSCs, fabricated using diverse morphologies and methods, vary widely, with values that are still relatively low [16-21]. To enhance the energy conversion efficiency of DSSCs, understanding the behavior of injected electrons in TiO_2 is crucial. This understanding is influenced by the structure and architectural development of TiO_2, as well as the thickness of the TiO_2 film. Efforts have been made to reduce recombination rates and increase the diffusion length of charge carriers [22], leading to significant scientific and engineering endeavors for optimization [23]. It is noteworthy that the enhancement of energy conversion efficiency is directly related to the light-scattering power of TiO_2. Larger particles, with relatively small surface areas and low absorption abilities for dyes, impact photo-irradiance efficiency [24, 25]. To enhance absorption ability and device parameters, various TiO_2 nano-composites with different architectures have been synthesized using diverse synthesis techniques.

In this chapter, we present an approach to creating a photosensitive TiO_2–ZnO nanocomposite with enhanced absorption compared to TiO_2 nanoparticles. This augmentation in absorption capability, coupled with a reduction in the optical band gap energy of the surfactant-guided synthesized TiO_2-ZnO composite, remains unexplored until now. The synthesized materials underwent characterization to discern their identities and distinguish them from each other. Following an examination of their optical behavior, these two materials were employed in the fabrication of a Dye Sensitized Solar Cell (DSSC). Our challenge was to boost the rate of carrier generation with effective mobility (μ_{eff}) and reduce recombination by enhancing absorption capability and modifying the band gap of the active materials, ultimately improving the DSSC's performance. The enhancement of DSSC efficiency by substituting TiO_2 with the TiO_2-ZnO nanocomposite is elucidated with arguments and supported by experimental evidence in this text.

2. Synthesis

In the standard TiO_2 synthesis procedure, 5 g of Titanium tetrachloride ($TiCl_4$) was combined with 100 ml of water, and the resulting solution was divided into two aliquot volumes. In a separate beaker, 0.5 g of Zinc acetate was dissolved in 50 ml of water. The first part of the stock solution was vigorously mixed with the Zinc acetate solution and stirred continuously. A pre-prepared 0.1N NaOH solution was then added drop by drop to the combined solutions while maintaining a pH of approximately 6-7, and the mixture was stirred for the next 2 hours. A few drops of polyvinyl pyrrolidone (PVP) were introduced as a capping reagent in both solutions. White precipitates were observed in both cases, and these were transferred into a linear Teflon autoclave and heated at 160°C for two days. After cooling to room temperature, the resulting white precipitate was washed repeatedly with deionized water and ethanol using a centrifuge technique. The sample was then collected as a powder after drying under vacuum at 100°C.

3. Material Characterization

The composite material's morphology was analyzed using Powder X-ray Diffraction (PXRD) with a Bruker D8 X-Ray Diffractometer and Transmission Electron Microscopy (TEM) using a JEOL JEM-1400 TEM. To identify functional groups, Fourier Transmission Infrared (FTIR) spectra were obtained using an FTIR-8400S Spectrophotometer from Shimadzu. UV-vis absorption spectra were recorded using a Shimadzu 2401PC spectrophotometer.

4. Interpretations

4.1. X-Ray Diffraction (XRD)

Figure 1 illustrates the powder X-ray diffraction (PXRD) spectra of (a) TiO_2 and (b) TiO_2-ZnO nanocomposite. The synthesis of TiO_2 and TiO_2-ZnO materials with phase identity was corroborated by JCPDS card No. 84-1286, 84-1750, and 36-1451. The average particle size was determined using the Scherrer's peak broadening equation, which considers the significant Bragg's diffraction peaks and their respective diffraction angles from the XRD spectra. Following the equation \(L = \frac{\lambda k}{B \cos\theta} \), the average particle size (L) was measured as 25 nm and 38 nm, respectively.

$$D = \frac{0.9\lambda}{B.cos\theta}$$

where, D is the crystallite size (nm), λ is the wavelength of the monochromatic X-Ray beam. We have considered here Cu as the target material for the production of X-Ray. The radiation wavelength (λ) of CuK_α was taken as = 0.15406 nm. B is the line broadening at half-maximum intensity of the diffraction peak and θ is the Bragg's angle. Here shape factor K was considered as 0.9.

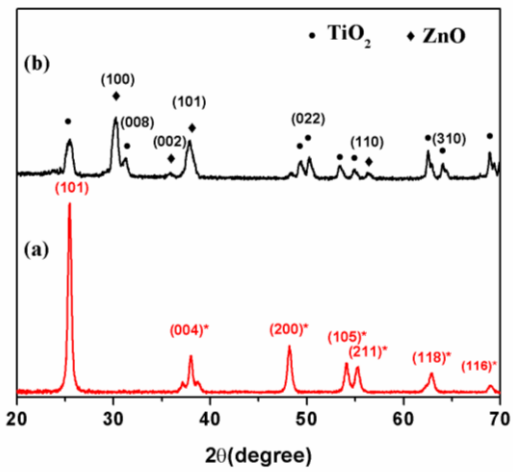

Figure 1: X-ray diffraction spectra of (a) TiO_2 and (b) TiO_2-ZnO nanocomposite.

4.2. Transmission Electron Microscopy (TEM)

Figure 2(a) and 2(b) illustrate the TEM images of TiO_2 and TiO_2-ZnO respectively, which exhibit that the sizes of the particles are in nanoscale. The crystalline of the particles are confirmed by Selected Area Electron Diffraction (SAED) patterns (Inset of Figure 2(a) and 2(b)):

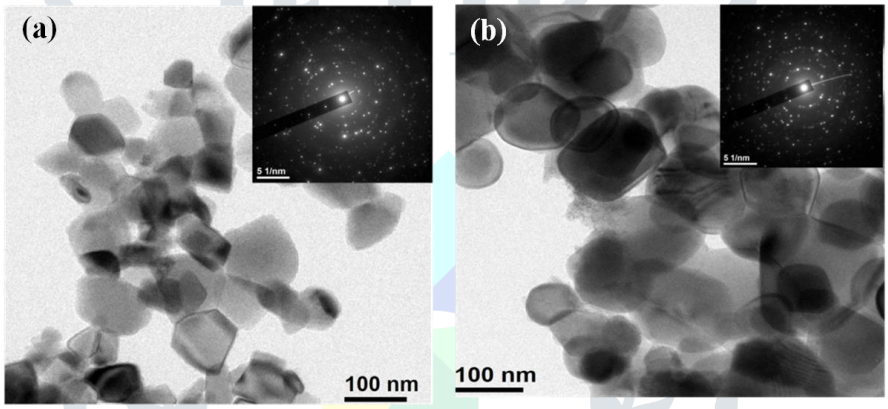

Figure 2: TEM images of (a) TiO_2 and (b) TiO_2-ZnO, (Inset a and b) SEAD images of TiO_2 and TiO_2-ZnO

4.3. Brunauer–Emmett–Teller (BET) Analysis

Figure 3 represents the BET surface area of TiO_2. TiO_2-ZnO powder were determined by nitrogen absorption at -196^{0}C by Quanta chrome Auto absorption analyzer (Quantachrome Instruments, USA).

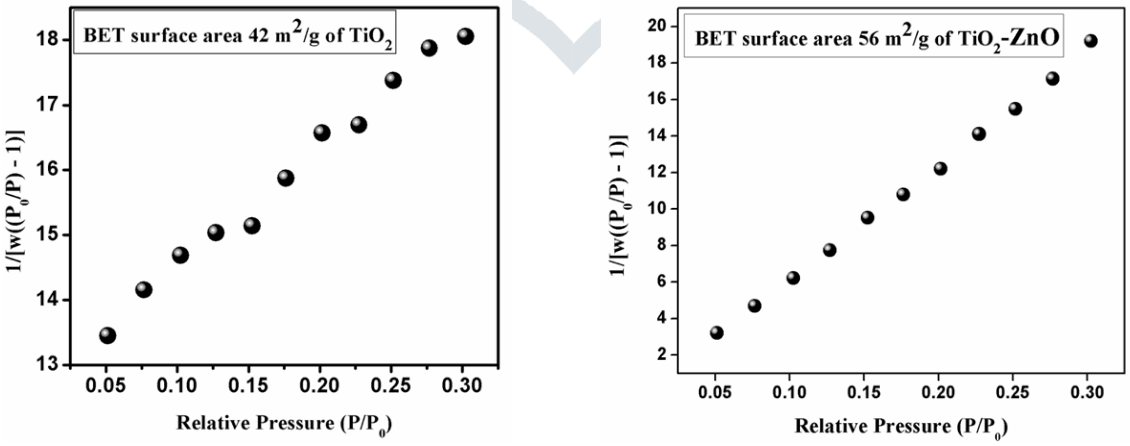

Figure 3: $1/[w((P_0/P)-1)]$ vs P/P_0 plot surface area of TiO_2 and TiO_2-ZnO

Before conducting nitrogen adsorption measurements, the samples underwent degassing at 100°C for 3 hours. Employing the BET equations and analyzing the slope and intercept of 1/[w((P0/P)-1)] vs P/P0 plots,

the surface area of TiO_2 and TiO_2-ZnO nanoparticles was determined to be 40 m2/g and 54 m2/g, respectively.

4.4. FTIR analysis

Figure 4 indicatees Fourier Transformed Infra-red (FTIR) spectra of TiO_2-ZnO composite, which shows a broad band around 400-600 cm^{-1}. This is attributed to Ti-O-Ti bridging stretching mode [26].

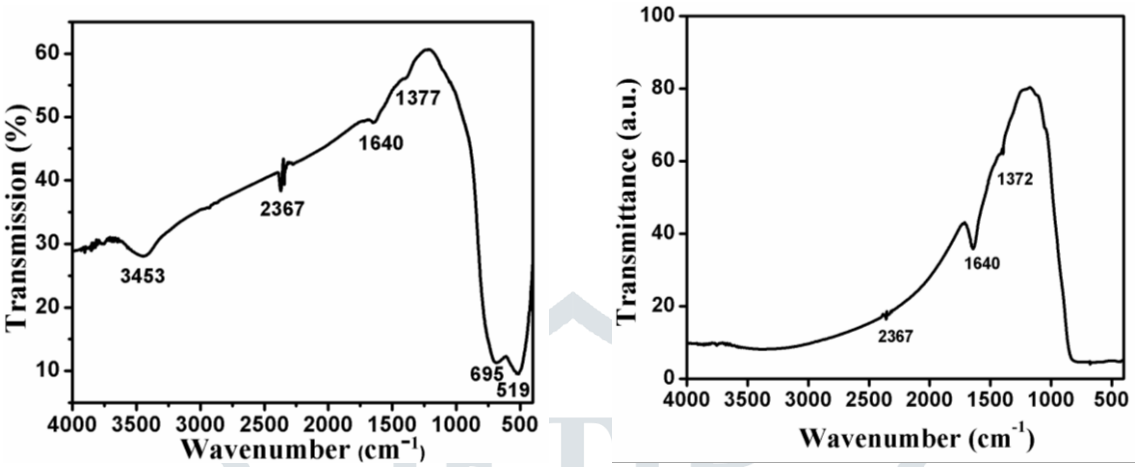

Figure 4: FTIR spectra of TiO_2-ZnO composite

Wavenumber 1377 cm^{-1} attributed to Ti-O stretching mode. The peak at 3453 cm^{-1} and 1640 cm^{-1} corresponds to stretching vibration of O-H and bending vibration of adsorbed water molecules respectively. A sharp strong band at 695 cm^{-1} was observed corresponding to stretching mode of Zn-O nanoparticles. With increase of Zn content, Ti-O band shifts to lower wavenumber region and gets sharpened.

4.5. TGA Analysis

The thermal stability of both TiO_2 and TiO_2-ZnO composite was investigated using the DTG-60 Thermogravimetric and Differential Thermal Analyzer from Shimadzu. The samples were individually heated at a rate of 100°C min-1 in a nitrogen atmosphere, and the thermal degradation of mass with decomposition was recorded within the temperature range of 100°C to 800°C (depicted in Figure 5). Initially, to eliminate moisture, the samples underwent heating at 100°C under a vacuum oven. The TGA curves reveal a noticeable weight loss between 100°C and 260°C for the TiO_2-ZnO composite material. This loss may be attributed to the decomposition of the condensation dehydration of the remaining hydroxyls. Subsequently, the degradation rates for both samples increased as the temperature rose, indicating the commencement of decomposition. The rate of degradation for of the TiO_2-ZnO nanocomposite is significantly higher compared to TiO_2. At a temperature of 800°C, the TiO_2 and TiO_2-ZnO composite samples were decomposed to 82% and 58% of their initial weight, respectively. The TGA curves clearly indicate that the TiO_2-ZnO composite experienced substantial weight loss due to its pronounced thermal degradation, highlighting its higher reactivity, while TiO_2exhibited greater thermal stability.

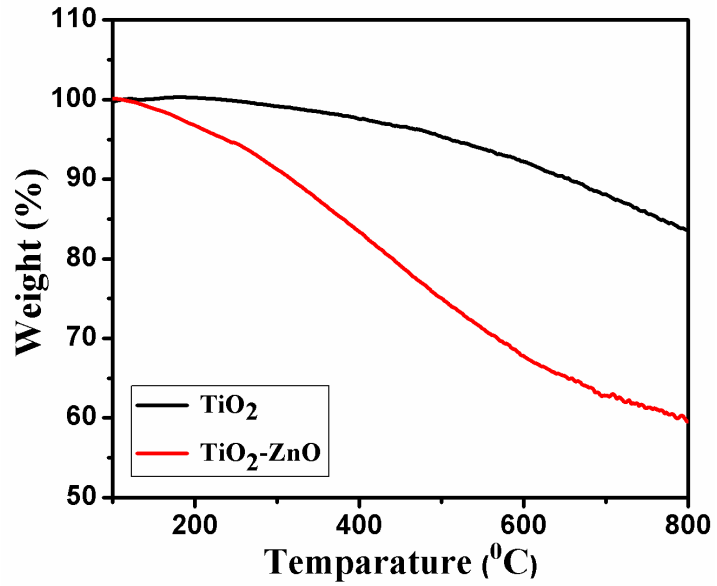

Figure 5: TGA spectra of TiO_2 and TiO_2-ZnO composite

4.6. UV-vis Absorption

Figure 6 depicts the UV-vis absorption spectra of TiO_2 and TiO_2-ZnO, revealing a significant shift in the absorption edge of TiO2 resulting from the incorporation of ZnO. The chemical growth rate of the nanomaterial is notably influenced by the surfactant's chain length and the chemical vapor pressure [27].

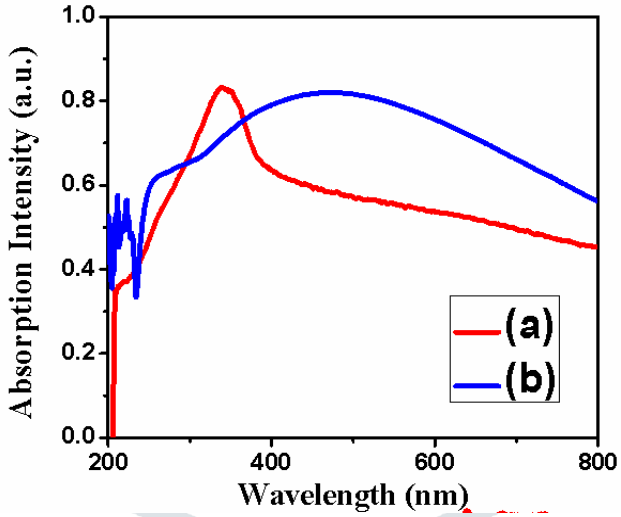

Figure 6: UV-vis absorption spectra of TiO_2(a) and TiO_2 –ZnO(b)

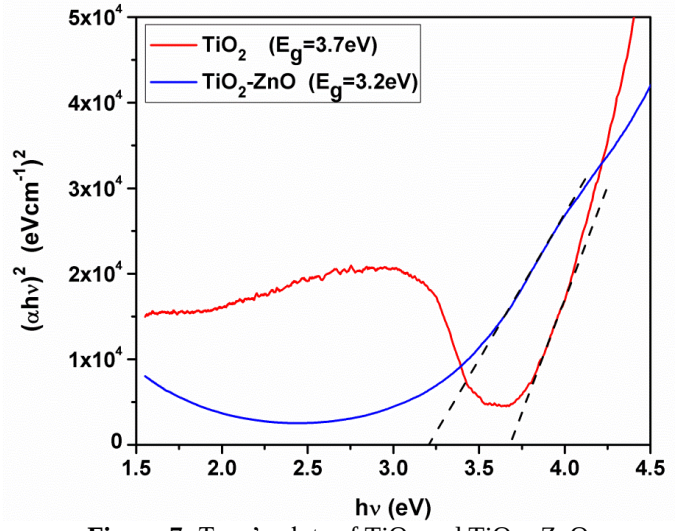

Figure 7: Tauc's plots of TiO_2 and TiO_2 –ZnO

As a consequence, there is an accumulation of more charge carriers in the valence band, ultimately leading to a reduction in the energy band gap. The optical energy band gaps were determined as 3.1 eV for TiO_2-

ZnO and 3.6 eV for TiO_2 (Figure 7) using Tauc's equation. Due to its lower band gap and higher absorption, the TiO_2-ZnO composite holds significance as a crucial material in Dye Sensitized Solar Cells (DSSCs).

5. Device Fabrication

Before device fabrication, slurries (colloids) of TiO_2 and TiO_2 -ZnO were prepared using the conventional method with acetonitrile. These slurries were subsequently coated onto pre-cleaned Indium Tin-Oxide (ITO) substrates and sintered at 120°C. Following the cooling to room temperature, the coated substrates were immersed in a solution of Brilliant Green dye, left overnight in a cold and dark environment. Excess dye was removed by rinsing with distilled water, and the films were dried at 120°C. The ITO-coated counter electrodes were then assembled and sealed in a sandwich-like structure. An aqueous solution of KI and I_2 was injected as the electrolyte into the active device.

6. Device Characterizations

6.1. Current-voltage characteristic

Figure 8 represents the current density vs. voltage (J - V) characteristics of DSSCs with configuration (a) ITO/TiO_2/Dye/I^{3-}/ITO and (b) ITO/TiO_2-ZnO/Dye/I^{3-}/ITO. DSSC based on TiO_2-ZnO nanocomposite exhibits high V_{oc} and slight increment in J_{sc} with

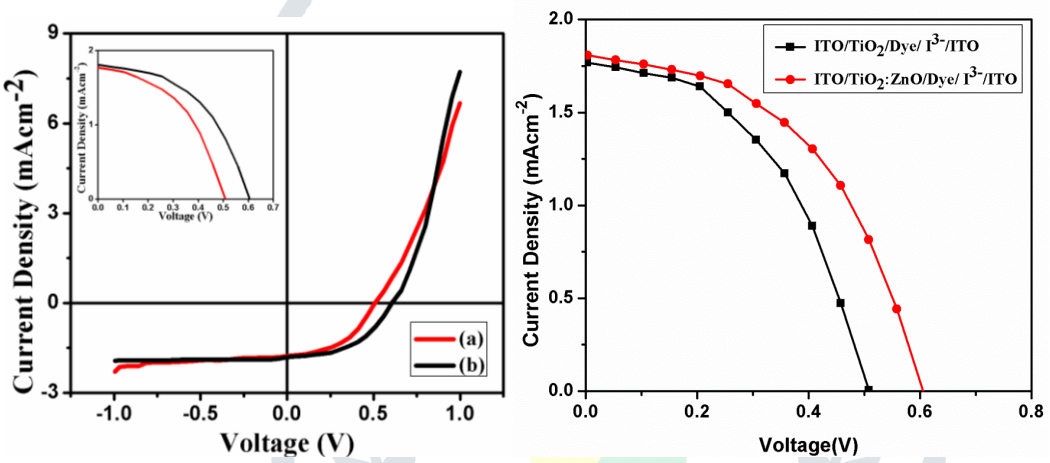

Figure 8: (J –V) characteristics of (a) ITO/TiO_2/Dye/I^{3-}/ITO and (b) ITO/TiO_2-ZnO/Dye/I^{3-}/ITO based device

improved efficiency and FF compared to the TiO_2 based one (Table I). With all these parameters along with lower R_s proves the overall improvement in the performance of TiO_2-ZnO based solar cell.

Table I: Characteristic parameters of the DSSCs

Device Configuration	J_{SC} (mAcm^{-2})	V_{OC} (Volt)	FF	Efficiency (%)	Rs (Ω)	L_D (nm)	μτ (cm^{2}V^{-1})
ITO/TiO_2/Dye/I_3^-/ITO	1.164	0.509	0.49	0.288	416	56	6.89×10^{-10}
ITO/TiO_2:ZnO/Dye/I_3^-/ITO	1.189	0.606	0.51	0.365	397	61.5	8.36×10^{-10}

We observed a substantial increase in Voc (from 508 mV to 605 mV) in the TiO_2-ZnO-based Dye Sensitized Solar Cell (DSSC), possibly due to the elevation of the Fermi energy level influenced by the doping composition of the synthesized material. The Voc is associated with charge recombination with either oxidized dye or tri-iodide electrolyte [28]. To gain further insights into the devices, we qualitatively analyzed charge transport properties using the Space-Charge-Limited-Current (SCLC) theory and the Einstein-Smoluchowski equation.

6.2. Estimation of mobility, time of flight and diffusion length of photogenerated charge carriers

The analysis of the charge transport mechanism in the devices was conducted through ln(J) vs. ln(V) plots, as depicted in Figure 9. These curves are indicative of space charge-limited current (SCLC) and recombination rate. The rate of recombination can be elucidated by its impact on the mobility of the carriers. From the ln(J) vs. ln(V) plot, we estimated the carrier diffusion length (LD) and the mobility-lifetime ($\mu\tau$) product. The carrier mobility was determined from the slope of the ln(J) vs. ln(V) plot using the Mott-Gurney space-charge-limited-current (SCLC) equation [29].

$$J = \frac{9\mu_{eff}\,\varepsilon_0\varepsilon_r}{8}\left(\frac{V^2}{d^3}\right)$$

where, J is the current density, ε_0 is the permittivity of free space, ε_r is the relative dielectric constant. The literature value of ε_r=2.9 for metal oxide semiconductor nanoparticles was employed [30, 31].

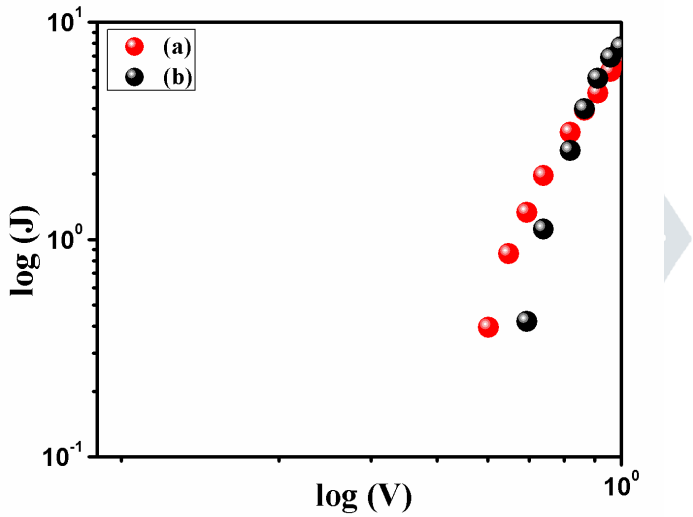

Figure 9: log(J) vs. log(V) characteristic of (a) ITO/TiO_2/Dye/I^{3-}/ITO and (b) ITO/ TiO_2-ZnO /Dye/I^{3-}/ITO DSSC

We also have the equation of charge carrier mobility:

$$\mu = \frac{d^2}{V\tau}$$

where, d is the distance between two electrodes i.e. the thickness of the film and τ is the transient time of the photogenerated charge carriers. From these two equations eliminating μ the time of flight can be illustrated as:

$$\tau = \frac{9\varepsilon_0\varepsilon_r}{8d}\left(\frac{V}{J}\right)$$

From the slope of characteristic J-V plot (Figure 10), considering the space charge limited current for the bias potential (> V_{oc}), the transient time was evaluated.

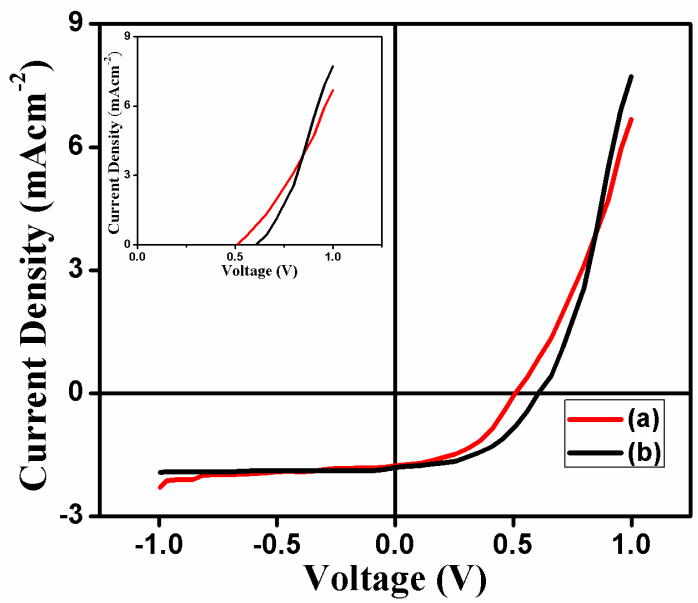

Figure 10: J-V characteristic of (a) ITO/TiO_2/Dye/I^{3-}/ITO and (b) ITO/ TiO_2-ZnO /Dye/I^{3-}/ITO

Moreover to calculate the diffusion length of the photogenerated charge carrier we have introduced Einstein-Smoluchowski equation:

$$\mu = \frac{qD}{K_B T}$$

where, D is the diffusion coefficient and T is the room-temperature in Kelvin scale.
From this equation calculating D values the diffusion length was estimated by the equation:

$$L_D = \sqrt{2D\tau}$$

From this analysis, we observe an increase in the carrier diffusion length (LD) and the mobility-lifetime (μτ) product (Table II) in the TiO_2-ZnO-based device, despite the material behaving as a resistive material. This affirms the enhancement of charge transport properties within the device, accompanied by a reduced rate of recombination. The fill factor (FF) and series resistance (Rs) of the TiO_2-ZnO-based device have improved, likely due to the enhancement of junction properties within the device.

Table-II

Device Configuration	V_{max} (Volt)	P_{max} (mWattcm^{-2})	μ (cm^{2}v^{-1}s^{-1})	τ (s)
ITO/TiO_2/Dye/I_3^-/ITO	0.36	0.288	1.45×10^{-7}	2.54×10^{-3}
ITO/TiO_2:ZnO/Dye/I_3^-/ITO	0.41	0.365	3.29×10^{-7}	4.75×10^{-3}

The above demonstration affirms the superiority of the novel TiO_2 -ZnO composite within Dye Sensitized Solar Cells (DSSC), paving the way for the fabrication of efficient devices with improved quality. The device's performance can potentially be further enhanced by optimizing the thickness of the active layer.

7. Summary

In this chapter, we introduced a novel technique for synthesizing a hierarchical TiO_2-ZnO nanocomposite with PVP surfactant and explored its subsequent application to enhance the overall performance of Dye Sensitized Solar Cells (DSSCs). A notable enhancement in the Voc of the TiO_2-ZnO nanocomposite-based device was achieved. Our approach aimed to tailor the material properties for optimal device performance through controlled growth facilitated by a suitable surfactant. Both quantitative and qualitative analyses highlight the superiority of the material, showcasing improved charge transport properties for effective device application.

References

[1] F. Gracia, J. P. Holgado, A. Caballero, A. R. Gonzalez-Elipe, *J. Phys. Chem. B* 108 (2004) 17466
[2] A. Mattsson, M.Leideborg, K. Larsson, G.Westin, L. J. Osterlund, *Phys. Chem. B* 110 (2006) 1210
[3] L. F. Fu, N. D. Browning, S. X. Zhang, S. B. Ogale, D. C. undaliya, T. J. Venkatesan, *Appl. Phys.* 100 (2006) 123910
[4] T. Umebayashi, T. Yamaki,; H.Itoh,; K.Asai, *Appl. Phys. Lett.* 81(2002) 454
[5] J. C.Yu, Z.Zheng, Zhao, *J. Chem. Mater.* 15 (2003) 2280
[6] C. J. Yu.; J. Yu.; W. Ho; Z. Jiang; L. Zhang *Chem. Mater.* 14 (2002) 3808

[7] B. Oregan, M. Gratzel, *Nature* 353 (1991) 737

[8] A. Hagfeldt, M. Gratzel, Chem. Rev. 95 (1995) 49

[9] H. N. Ghosh, *J. Chem. Sci.* 119 (2007) 205

[10] A. Zaban, S. G. Chen., S. Chappel, B. A. Gregg, Chem. Comm. 134 (2000) 2231

[11] B. A. Gregg, F. Pichot, S. Ferrere, C. L. Fields, *J. Phys. Chem. B.* 105 (2001) 1422

[12] S.J. Roh, R.S. Mane, S.K. Min, W.J. Lee, C.D. Lokhande, S.H. Han, *Appl Phys Lett*, 89 (2006) 253512
[13] W. Yang, F. Wan, S. Chen, C. Jiang, *Nanoscale Res. Lett.* 4 (2009) 1486
[14] S. Rani, P. Suri, P. K. Shishodia and R. M. Mehra, *Sol. Energy Mater. Sol. Cells* 92 **(**2008) 1639
[15] Y. Chiba, A. Islam, Y. Watanabe, R. Komiya, N. Koide and L. Han, Jpn. *J. Appl. Phys.*45 (2006) 638.
[16] L. Yang, Y. Lin, J. Jia, X. Xiao, X. Li and X. J. Zhou, *J. Power Sources* 182 (2008) 370
[17] H. J. Koo, Y. J. Kim, Y. H. Lee, W. I. Lee, K. Kim and N. G. Park, *Adv. Mater.* 20 (2008) 195
[18] A. Mihi, M. E. Calvo, J. A. Anta and H. J. Miguez, *J. Phys. Chem.C* 112 (2008) 13
[19] S. Hore, P. Nitz, C. Vetter, C. Prahl, M. Niggemann and R. Kern, *Chem. Commun.* 15 (2005) 2011
[20] Y. J. Kim, M. H. Lee, H. J. Kim, G. Lim, Y. S. Choi, N. G. Park, K. Kim and W. I. Lee, *Adv. Mater.* 21 (2009) 1
[21] F. Pichot and B. A. Gregg, *J. Phys. Chem. B* 104 (2000) 6
[22] K.J. Hwang, C. Im, D. W. Cho, S.-J. Yoo, J.-W. Lee and W.-G. Shim, *RSC Adv.* 2 (2012) 3034
[23] M. Grätzel, *Nature* 414 (2001) 338
[24] S. Ito, T. N. Murakami, P. Comte, P. Liska, C. Gratzel, M. K. Nazeeruddin and M. Gratzel, *Thin Solid Films* 516 (2008) 4613
[25] P. Wang, S. M. Zakeeruddin, P. Comte, R. Charvet, R. Humphy-Baker and M. Gratzel, *J. Phys. Chem.B* 107 (2003) 14336
[26] J.Tian, L. Chen, Y. Yin, X. Wang, J. Dai, Z. Zhu, X. Liu, P. Wu, *Surface & Coatings Technology* 204 (2009) 205

[27] X. Chen, S.S. Mao, *Chem. Rev.* 107 (2007) 2891

[28] S. J. Roh, R. S. Mane, S. K. Min, W. J. Lee, C. D. Lokhande, S. H. Han, *Appl. Phys. Lett.* 89 (2006) 253512

[29] P. W. M. Blom, M. Jong . J. M. de, M. G. V. Munster, *Phys. Rev. B: Condens. Mater.* 55 (1997) 656

[30] M. Schidleja, C. Melzer, H. V. Seggern, *Adv. Mater.* 21 (2009) 1172

[31] J.S. Park, J. M. Lee, S. K. Hwang, S. H. Lee, H. J. Lee, B. R. Lee, H. I. Park, J. S. Kim, S. Yoo, M. H. Song, S. O. Kim, *J. Mater. Chem.* 22 (2012) 12695